Journal of Materials Chemistry A

ROYAL SOCIETY OF CHEMISTRY

PAPER

View Article Online
View Journal | View Issue

Cite this: J. Mater. Chem. A, 2023, 11, 23922

Post-synthetic modification of zeolitic imidazolate framework-90 *via* Schiff base reaction for ultrahigh iodine capture†

Zilong Zhang,‡[a] Yanchun Chen,‡[a] Yiheng Sun,[a] Zilu Chen,*[a] Zhan-Yun Zhang,*[a] Fupei Liang,[ab] Dongcheng Liu[a] and Huan-Cheng Hu*[a]

Received 6th August 2023
Accepted 12th October 2023

DOI: 10.1039/d3ta04686a

rsc.li/materials-a

The post-synthetic modification of zeolitic imidazolate frameworks (ZIFs) is an effective strategy for preparing new materials that exhibit superior performance compared to their parental ZIFs. Herein, we quantitatively transformed the aldehyde group of **ZIF-90** into mono- and bis-Schiff bases, and the resulting compounds **ZIF-90-I–ZIF-90-III** still retained the crystallinity and their parental structures. Importantly, **ZIF-90-III** with the highest amount of mono-Schiff base showed the maximum iodine uptake capacities of 6600 mg g^{-1} and 1826 mg g^{-1} for iodine vapor and iodine/cyclohexane solution, respectively, which are 1.5- and 3.4-fold as much as that of **ZIF-90**, being among the highest reported to date for metal–organic frameworks (MOFs). Noteworthily, activation energies for iodine adsorption of **ZIF-90** and its post-synthetic derivatives were speculated experimentally, which was firstly investigated for MOFs. Meanwhile, adsorption kinetics, iodine species during iodine adsorption process and the related theoretical calculations were also studied in detail.

1 Introduction

Nuclear energy is regarded one of excellent candidates to replace fossil energy because of its high efficiency and non-carbon-emission.[1,2] However, nuclear waste pollutants, such as numerous volatile radionuclides ^{3}H, ^{85}Kr, ^{129}I and ^{131}I, are inevitably generated during the process of fuel fission, which damage the ecosystem and bring serious harm to humans and animals once they are accidently leaked.[3] Among the above-mentioned pollutants, radioactive iodine has obtained world-wide interest, because both the long-lived ^{129}I ($t_{1/2} = 1.57 \times 10^{7}$ years) and short-lived ^{131}I ($t_{1/2} = 8.02$ days) can affect human metabolic processes, further leading to thyroid cancer and hypothyroidism.[4] However, the low solubility and easy mobility of iodine make it difficult to capture.[5,6] Thus, the adsorption of iodine is an urgent and challenging worldwide issue.

In the past decades, many porous materials, such as silver-exchanged zeolite, mesoporous silica, porous organic cages, covalent organic frameworks, and metal–organic frameworks, have been reported to trap iodine.[7–11] Among these materials, MOFs are viewed as an outstanding candidate for iodine adsorption owing to its high surface area, suitable pore size and good chemical and thermal stability. The zeolitic imidazolate framework (ZIF) is a very important subfamily of metal–organic frameworks. Previously reported studies identified that a charge-transfer complex was modestly formed between the electron-deficient iodine molecule and electron-rich aromatic carbon molecules in them; therefore, ZIFs often exhibited high iodine adsorption amounts. For example, **ZIF-8** showed a good iodine vapor adsorption capacity of 1.25 g g^{-1} at 350 K under ambient pressure,[12,13] and the iodine adsorption amount of single particle **ZIF-90** with a size of 3.8 μm is 220 mg g^{-1} within 180 s at room temperature.[14] Additionally, the high electron density of organic linkers usually contributes to generating strong interactions between the iodine molecule and framework. This further leads to extraordinary iodine adsorption capacities of the materials. Hence, the introduction of rich electron groups (such as C=N/C=C/C≡C with π electron and OH/NH_2 with a lone pair electron) and organic linker defects were regarded as an effective strategy to increase the electron density of the organic ligands. For example, the iodine vapor adsorption amount of **UiO-67** was 530 mg g^{-1}, while the values were increased up to 1071 mg g^{-1} and 1211 mg g^{-1} for **UiO-67-NH_2** and **UiO-67-$(NH_2)_2$**, respectively.[15,16] When organic linker defects were anchored to **ZIF-90**, the partial broken Zn–N bonds decreased the delocalization of N atoms from imidazole-2-carboxaldehyde, and the electron density of the aromatic ring

[a]School of Chemistry and Pharmaceutical Sciences, State Key Laboratory for Chemistry and Molecular Engineering of Medicinal Resources, Guangxi Normal University, Guilin, 541004, People's Republic of China. E-mail: zlchen@mailbox.gxnu.edu.cn; zhang_zhanyun@126.com; siniantongnian@126.com

[b]Guangxi Key Laboratory of Electrochemical and Magnetochemical Functional Materials, College of Chemistry and Bioengineering, Guilin University of Technology, Guilin, 541004, People's Republic of China

† Electronic supplementary information (ESI) available: PXRD patterns, IR spectra, ^{1}H NMR, HRESI-MS, UV-vis absorption spectra, *etc.* See DOI: https://doi.org/10.1039/d3ta04686a

‡ These authors contributed equally to this work.

from imidazole was increased, so the iodine adsorption amount of single **ZIF-90** particle was significantly improved to 400 mg g^{-1} at the same condition.[14] However, the introduction of rich electron groups with both π electron and lone pairs in MOFs has rarely been reported except for the core–shell **NH_2-UiO-66@Br-COFs** hybrid material, in which the maximum iodine vapor adsorption amount was up to 3.73 g g^{-1} at 75 °C and obviously superior to that of **NH_2-UiO-66** (565 mg g^{-1}).[16,17]

In this context, we chose **ZIF-90** with aldehyde groups as the precursor and reacted it with 1,2-diaminocyclohexane. The aldehyde groups of **ZIF-90** were consequently converted into mono- and bis-Schiff bases, and both C=N and NH_2 groups were introduced in **ZIF-90** for improving the electron density of aromatic ring. A series of post-synthetic functionalizations of **ZIF-90** derivatives (**ZIF-90-I–ZIF-90-III**) were prepared *via* controlling the molar ratio of **ZIF-90** and 1,2-diaminocyclohexane. Moreover, iodine adsorption experiments of these materials were also carried out by means of weighting method for iodine vapor and monitoring on a UV-vis spectrometer for iodine/cyclohexane solution, respectively. Activation energies, adsorption kinetics, iodine species and related theoretical analysis of **ZIF-90** and its post-synthetic derivatives during iodine adsorption process were also investigated.

2 Experiment

2.1. Materials and methods

All reagents in our research study were purchased from commercial sources and used without further purification. Powder X-ray diffraction (PXRD) patterns were obtained using a D/Max-3c X-ray diffractometer (Rigaku, Japan) with Cu Kα radiation. Fourier transform infrared spectroscopy (FTIR) spectra were collected using a Spectrum Two spectrometer (PerkinElmer, USA). ^{1}H NMR spectra were measured on a Bruker Avance III HD 400 MHz spectrometer (Bruker, Germany). High-resolution electrospray ionization mass spectrometry (HRESI-MS) measurements were obtained on an Exactive mass spectrometer (Thermo Fisher Scientific, Germany). N_2 adsorption isotherm measurements were performed on a BELSORP-max II adsorption apparatus (BEL, Japan) at 77 K. Scanning electron microscopy (SEM) was performed on a TESCAN MIRA LMS (TESCAN, Czech Republic). UV-vis absorption spectra were obtained on a CARY ECLIPSE JASCO-720 spectrophotometer (Agilent, USA). Raman spectra were obtained on a Renishaw Invia Raman spectrometer (Invia, UK). X-ray photoelectron spectra (XPS) were conducted on a Physical Electronics Model 5400 X-ray photoelectron spectrometer using an unmonochromatized Mg Kα X-ray source.

2.2. Synthetic procedures

2.2.1 Synthesis of (*E*)-2-(((1*H*-imidazol-2-yl)methylene) amino)cyclohexan-1-amine (L^2, denoted mono-Schiff base). 1,2-Diaminocyclohexane (114.2 mg, 1.0 mmol) was dissolved in MeOH (20 mL) in a 100 mL flask. 1 M hydrochloric acid (1.1 mL) was slowly added to this solution and then stirred for 20 minutes. The solution of imidazole-2-carboxaldehyde (L^1, 96.0 mg, 1.0 mmol) in MeOH (10 mL) was slowly added to the above system, and then the mixture was refluxed overnight. Finally, the resulting suspension was adjusted to a pH of ~8.0 by the saturated $NaHSO_3$ aqueous solution (Scheme S1†). The product was further purified by recrystallization using MeOH.

2.2.2 Synthesis of (1*E*,1′*E*)-*N*,*N*′-(cyclohexane-1,2-diyl)bis(1-(1*H*-imidazol-2-yl) methanimine) (L^3, denoted bis-Schiff base). 1,2-Diaminocyclohexane (114.2 mg, 1.0 mmol) and imidazole-2-carboxaldehyde (192.0 mg, 2.0 mmol) were dissolved in MeOH (40 mL) in a 100 mL flask, and the mixture was refluxed overnight (Scheme S2†). The resulting product was obtained by filtration, and washed with fresh methanol.

2.2.3 Synthesis of ZIF-90. **ZIF-90** was prepared according to the previously reported procedure.[18] A mixture of imidazole-2-carboxaldehyde (96.0 mg, 1.0 mmol) and sodium formate (17.0 mg, 0.25 mmol) was added in MeOH (10 mL), and then sonicated for 20 minutes to form a clear yellow solution, followed by the addition of $Zn(NO_3)_2 \cdot 6H_2O$ (74.4 mg, 0.25 mmol). The obtained solution was transferred into a Teflon-lined stainless steel autoclave, and kept in an oven at 353 K for 24 h. The autoclave was then taken out and cooled to room temperature. The polyhedral crystals were collected by filtration, washed with fresh methanol, and then dried under vacuum at 373 K for one day.

2.2.4 Synthesis of ZIF-90-I–ZIF-90-III. The synthetic routes of **ZIF-90-I–ZIF-90-III** are briefly described in Scheme 1.

2.2.5 Synthesis of ZIF-90-I. **ZIF-90** crystals (50.0 mg) and 1,2-diaminocyclohexane (46.0 mg) were suspended in ethoxyethane (10 mL), and stirred overnight at room temperature. The powder was then centrifuged and washed with fresh ethoxyethane (3 × 10 mL) before being immersed in fresh methanol (20 mL) for two days. The powder was finally collected by filtration, and then dried under vacuum at 373 K for one day. Molar ratio of $L^1 : L^2 : L^3 = 67.6\% : 25.7\% : 6.7\%$.

2.2.6 Synthesis of ZIF-90-II. The method of preparing **ZIF-90-II** is similar to the procedure of **ZIF-90-I**, except that 120.0 mg 1,2-diaminocyclohexane was used. Molar ratio of $L^1 : L^2 : L^3 = 8.8\% : 58.4\% : 32.7\%$.

2.2.7 Synthesis of ZIF-90-III. The method of preparing **ZIF-90-III** is similar to the procedure of **ZIF-90-I**, except that 250.0 mg 1,2-diaminocyclohexane was used. Molar ratio of $L^1 : L^2 : L^3 = 1.0\% : 96.1\% : 2.9\%$.

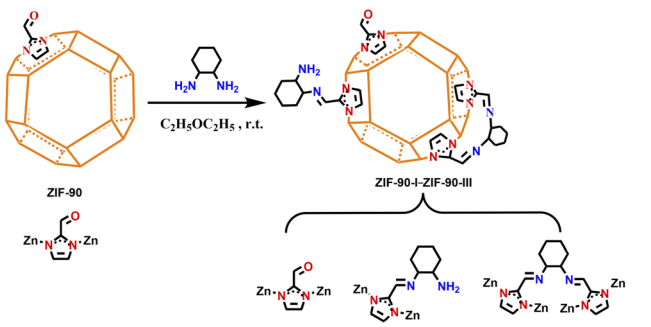

Scheme 1 Transformation of ZIF-90 by Schiff base reaction with 1,2-diaminocyclohexane to obtain ZIF-90-I–ZIF-90-III.

2.3. Iodine adsorption and desorption experiments

The iodine vapor adsorption experiments of **ZIF-90** and **ZIF-90-I–ZIF-90-III**. 10 mg of activated **ZIF-90** was placed in a pre-weighed 2 mL glass vial, and this glass vial was then put in a 20 mL sealed vial containing 300 mg of iodine pills, followed by being heated in an oven at 75 °C under ambient pressure. After a scheduled time, the iodine-loaded **ZIF-90** was cooled down to room temperature in a desiccator and then weighed. The colorless **ZIF-90** samples became dark brown. The iodine vapor adsorption experiments of **ZIF-90-I–ZIF-90-III** are similar to the adsorption process of **ZIF-90**, except that **ZIF-90** is replaced by **ZIF-90-I–ZIF-90-III**, respectively.

The iodine adsorption experiments of **ZIF-90** and **ZIF-90-I–ZIF-90-III** from iodine/cyclohexane solution. 5 mg of activated **ZIF-90** was soaked in 5 mL of iodine/cyclohexane solution with different concentrations (200–800 mg L^{-1}) under magnetic stirring at room temperature. The colorless **ZIF-90** samples became dark brown, while the purple iodine/cyclohexane solution faded to colorless with increasing time. After a certain time, the supernatant was collected by centrifugal separation and its absorbance was monitored by a UV-vis spectrophotometer. Additionally, in order to obtain the maximum iodine adsorption amount of **ZIF-90** in iodine/cyclohexane solution, 5 mg of activated **ZIF-90** was soaked in 15 mL of 500, 700 and 1000 mg L^{-1} iodine/cyclohexane solution, and the abovementioned procedure was performed. The iodine adsorption experiments of **ZIF-90-I–ZIF-90-III** in iodine/cyclohexane solution are similar to the adsorption process of **ZIF-90**, except that **ZIF-90** is replaced by **ZIF-90-I–ZIF-90-III**, respectively.

The iodine desorption experiments of iodine-loaded **ZIF-90** and **ZIF-90-I–ZIF-90-III**. 10 mg of iodine-loaded **ZIF-90** was placed in a pre-weighed 2 mL glass vial at 120 °C under ambient pressure. After a certain time, the glass vial was cooled down to room temperature in a desiccator and then weighed. The dark brown iodine-loaded **ZIF-90** samples faded over time. The iodine desorption experiments of iodine-loaded **ZIF-90-I–ZIF-90-III** are similar to the desorption process of iodine-loaded **ZIF-90**, except that iodine-loaded **ZIF-90** was replaced by iodine-loaded **ZIF-90-I–ZIF-90-III**, respectively.

3 Results and discussion

3.1. Characterization of ZIF-90-I–ZIF-90-III

The structures of **ZIF-90-I–ZIF-90-III** were characterized by powder X-ray diffraction (PXRD) and Fourier transform infrared spectroscopy (FTIR) measurements. As shown in Fig. S1,† the PXRD patterns of **ZIF-90-I–ZIF-90-III** are in agreement with the ones of experimental and simulated **ZIF-90** generated from single crystal X-ray diffraction data, indicating that **ZIF-90-I–ZIF-90-III** retained the crystallinity of **ZIF-90**, and no crystal impurities were introduced during the post-synthetic modification procedure. The FTIR spectrum showed the presence of a C=O stretching vibration at 1680 cm^{-1} for **ZIF-90**, whereas there was the appearance of a C=N stretching vibration at 1640 cm^{-1} for **ZIF-90-I–ZIF-90-III**, indicating the transformation from the aldehyde group to Schiff bases of **ZIF-90**. Additionally, the features at 3300 and 3144 cm^{-1} can be assigned to the symmetric and asymmetric NH_2 stretching vibrations, 2928 cm^{-1} belongs to the CH/CH_2 stretching vibrations, 1581 cm^{-1} is attributed to the in-plane NH_2 vibrations and the out-of-plane NH_2 vibrations are situated in the 940–770 cm^{-1} region (Fig. S2†).[19,20] These characteristics also revealed that 1,2-diaminocyclohexane has been anchored on **ZIF-90** *via* the Schiff base reaction. Additionally, the N_2 adsorption isotherms of the activated samples of **ZIF-90** and **ZIF-90-I–ZIF-90-III** were recorded at 77 K (Fig. S3†). The very low N_2 uptakes of **ZIF-90-I–ZIF-90-III** relative to that of **ZIF-90** may be attributed to an obvious constriction of the pores,[21] resulting from the conversion of the small size aldehyde to the bigger size Schiff bases. The SEM images showed that the morphology of **ZIF-90** was changed from a polyhedron to an irregular shape because of the post-synthetic modification. **ZIF-90-I–ZIF-90-III** exhibited almost the same particle size, which is obviously smaller than that of **ZIF-90** (Fig. S4†). A smaller particle size of the materials generally leads to a higher gas adsorption capacity, but **ZIF-90-I–ZIF-90-III** presented a lower N_2 adsorption capacity. Thus, the constriction of the pore through turning the aldehyde groups into Schiff bases probably played a major role in N_2 adsorption.

In order to confirm the quantitative conversion from the aldehyde group of **ZIF-90** to mono- and bis-Schiff bases (L^2 and L^3), activated **ZIF-90-I–ZIF-90-III** (10.0 mg) was put into 3 mL of MeOH to form a suspension under stirring. This mixture was then digested *via* the addition of 10% HCOOH/MeOH to adjust to a final pH of 5–6. The clear solution was evaporated and the resulting powder was dissolved in DMSO-d_6 to measure ^1H NMR, respectively. As shown in Fig. S5–S8,† the ^1H NMR spectra of the digested **ZIF-90-I–ZIF-90-III** samples show that resonances occur at around 8.32, 8.15 and 8.04 ppm, which correspond to the imidazole-2-carboxaldehyde, mono- and bis-Schiff bases, indicating that approximately 32.4%, 91.2% and 99% conversion of the aldehyde group had been completed in **ZIF-90-I–ZIF-90-III**, respectively. The neighboring distance of the aldehyde groups in **ZIF-90** is around 4.3 Å, which is close to the sum of the N…N distance from 1,2-diaminocyclohexane and C=N distance from the Schiff base. Thus, the aldehyde groups in **ZIF-90** can be converted to bis-Schiff bases during the process of post-synthetic modification. However, the transformation of the bis-Schiff base is not very high (~30%) owing to the steric hindrance effect. Meanwhile, we also carried out high-resolution electrospray ionization mass spectrometry (HRESI-MS) on these digested samples of **ZIF-90-I–ZIF-90-III**. As depicted in Fig. S9–S12,† compared with the HRESI-MS of the digested **ZIF-90**, four new *m*/*z* peaks were clearly observed for the digested **ZIF-90-I–ZIF-90-III** samples at 255.06, 273.06, 301.06 and 333.09, respectively. Fitting these peaks gives a formula of $[Zn(L^2)]^+$ (calcu. 255.06), $[Zn(L^2)(H_2O)]^+$ (calcu. 273.07), $[Zn(L^2)(HCOOH)]^+$ (calcu. 301.06) and $[Zn(L^3)]^+$ (calcu. 333.08) (Fig. S13†). The existence of these *m*/*z* peaks relevant to L^2 and L^3 fragments also provided further evidence for the transformation from aldehyde group of **ZIF-90** to Schiff bases. The speculated chemical formulae of the fragments are listed in Tables S1–S4.†

3.2. Iodine vapor capture of ZIF-90-I–ZIF-90-III

ZIFs such as **ZIF-8** and **ZIF-90** with suitable cage sizes and excellent chemical and thermal stability, easily form charge-transfer compounds between the iodine molecule and framework. Thus, they are viewed as ideal candidates for trapping iodine.[11–13] Meanwhile, the introduction of C=N with a π electron and NH_2 group featuring a lone pair electron will increase the electron density of the organic linkers and further enhances the iodine…framework interactions, leading to the improvement of the iodine adsorption amount. Iodine vapor capture experiments were performed on activated samples of **ZIF-90** and **ZIF-90-I–ZIF-90-III** at 75 °C under ambient pressure. The iodine adsorption isotherms of these samples were depicted according to the equation of $Q_t = 1000 \times (m_t - m_0)/m_0$, respectively, where Q_t (mg g^{-1}) is the adsorption amount of iodine vapor per gram of sample at time t, m_0 (mg) is the initial mass of sample and m_t (mg) is the mass of the sample after adsorption at time t.

As shown in Fig. 1a, the time of iodine adsorption equilibrium was about 60 hours with excellent iodine adsorption capacity values of 4490, 5270, 5680 and 6600 mg g^{-1} for **ZIF-90** and **ZIF-90-I–ZIF-90-III**, respectively. The iodine adsorption capacity of **ZIF-90-III** is 1.5-fold that of **ZIF-90.** Interestingly, the iodine vapor adsorption capacities were enhanced with the increasing conversion of aldehyde to Schiff base, especially with the increasing ratio of mono-Schiff base. In addition, **ZIF-90-I–ZIF-90-III** possessed the approximate particle sizes, but they exhibited different iodine adsorption capacities, revealing that maybe the particle sizes did not distinctly affect the iodine adsorption of the **ZIF-90** derivatives. Therefore, the iodine adsorption behavior of **ZIF-90** and **ZIF-90-I–ZIF-90-III** indicates that not only suitable cage sizes and charge-transfer interaction between the iodine molecule and aromatic imidazole ring play an important role in iodine vapor adsorption, but the presence of C=N with the π electron and NH_2 group with the lone pair electron also contributes to increasing interactions between the electron-deficient iodine molecule and framework, thus leading to the obvious increase of iodine adsorption in post-synthetic **ZIF-90** derivatives. To our best knowledge, compared to the previously reported metal–organic frameworks (Fig. 1b and Table S5†), the iodine vapor adsorption capacities of **ZIF-90** and **ZIF-90-I–ZIF-90-III** are only lower than that of **IL@PCN-333** (Al) (7350 mg g^{-1})[22] and obviously superior to those of most MOFs, such as **PCN-333** (Al) (4420 mg g^{-1}),[23] **UPC-158-HCl** (2920 mg g^{-1}),[24] *etc.* Noteworthily, the iodine vapor adsorption value of **ZIF-90-III** ranks second among the reported MOFs under the same conditions to date.

To further investigate the iodine adsorption behavior of **ZIF-90** and **ZIF-90-I–ZIF-90-III**, iodine vapor adsorption experiments of these materials were carried out at different temperatures (40, 50, 60 and 90 °C) under ambient pressure, respectively, and their corresponding iodine adsorption isotherms and the equilibrium adsorption amounts were obtained (Fig. S14 and Table S6†). For **ZIF-90** and **ZIF-90-I–ZIF-90-III**, the times of iodine adsorption equilibrium were obviously shortened, while the iodine adsorption capacity values were significantly enhanced with increasing temperature. Furthermore, the iodine adsorption capacity of **ZIF-90-II** and **ZIF-90-III** at 90 °C is slightly lower than that at 75 °C.

Meanwhile, the pseudo-first and pseudo-second order kinetic models were adopted to probe the iodine adsorption kinetics of **ZIF-90** and **ZIF-90-I–ZIF-90-III**, and the corresponding kinetic equations were listed as follows:

$$\text{Pseudo-first order kinetic model: } Q_t = Q_e - Q_e \times e^{-k_1 t}$$

$$\text{Pseudo-second order kinetic model: } t/Q_t = 1/k_2 Q_e^2 + t/Q_e$$

where k_1 (h^{-1}) and k_2 (g mg^{-1} h^{-1}) are the pseudo-first and pseudo-second order rate constants, respectively, Q_t (mg g^{-1}) and Q_e (mg g^{-1}) are respectively the adsorption amount of iodine vapor by per gram of sample at time t and equilibrium. As depicted in Fig. 2 and S15–S23,† and according to the correlation coefficients (R^2) and calculated value of Q_e (mg g^{-1}) obtained by the pseudo-first and pseudo-second order kinetic equations at different temperatures (Tables S7–S10†), the iodine vapor adsorption of **ZIF-90** can be described by the pseudo-first order kinetic equation, indicating that the diffusion of the iodine molecule *via* pores was the rate-controlling

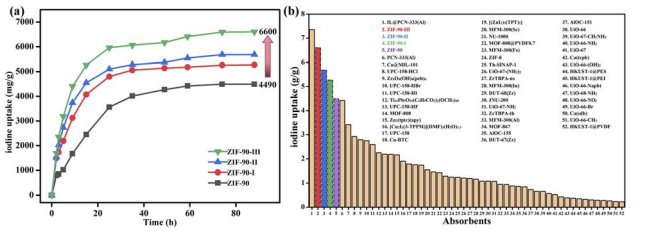

Fig. 1 (a) Iodine adsorption isotherms of ZIF-90 and ZIF-90-I–ZIF-90-III at 75 °C under ambient pressure, and (b) comparison of the iodine vapor adsorption capacity by reported metal–organic frameworks and our materials.

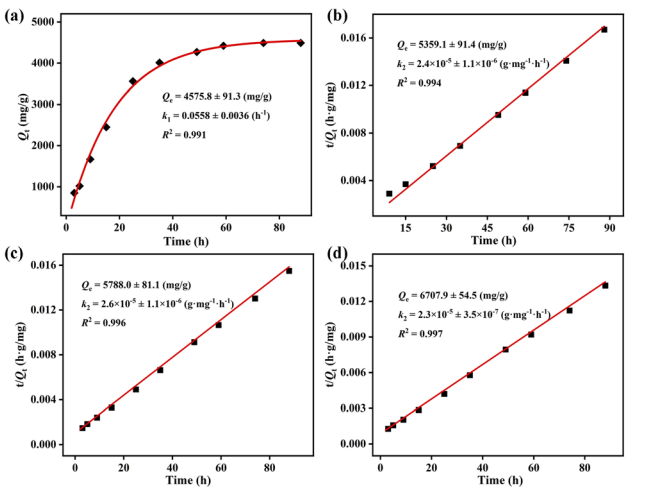

Fig. 2 (a) The pseudo-first kinetic model for the iodine vapor adsorption kinetics of ZIF-90, the pseudo-second kinetic models for the iodine vapor adsorption kinetics of (b) ZIF-90-I, (c) ZIF-90-II and (d) ZIF-90-III at 75 °C under ambient pressure.

mechanism for iodine vapor adsorption by **ZIF-90**.[25,26] While the pseudo-second order kinetic equation better favored the iodine vapor adsorption by **ZIF-90-I–ZIF-90-III**, revealing that chemisorption is predominant during the absorption progress for these post-synthetic **ZIF-90** derivatives.[27,28] Meanwhile, the order rate constants of k_1 and k_2 obviously increased with increasing temperature, probably ascribed to the more mobile iodine at higher temperature.

The Arrhenius equation $k = A\exp(-E_a/RT)$ was adopted to calculate the activation energy (E_a) during the iodine vapor adsorption process by **ZIF-90** and **ZIF-90-I–ZIF-90-III**, where k is the pseudo-first order rate constant for **ZIF-90** and the pseudo-second order rate constant for **ZIF-90-I–ZIF-90-III**, respectively, A is the pre-exponential factor, $R = 8.314$ J mol^{-1} K^{-1} and T is the Kelvin temperature. As shown in Fig. 3, the values of activation energy are 34.2 ± 1.5, 25.2 ± 0.9, 24.0 ± 0.9 and 23.1 ± 0.8 kJ mol^{-1} for **ZIF-90** and **ZIF-90-I–ZIF-90-III**, and all of them are lower than 40 kJ mol^{-1}. The lower activation energy implies the quicker diffusion of the iodine molecule, further leading to the high iodine adsorption capacity.[29,30] Thus, the sequence of the iodine vapor adsorption amount was **ZIF-90-III** > **ZIF-90-II** > **ZIF-90-I** > **ZIF-90**, which is coincident with the experimental values.

3.3. Iodine adsorption from iodine/cyclohexane solution by ZIF-90-I–ZIF-90-III

To determine the iodine adsorption capacity of **ZIF-90** and **ZIF-90-I–ZIF-90-III** in the iodine/cyclohexane solution, the standard curve of the iodine/cyclohexane solution was also measured (Fig. S24†). The absorbance at 522 nm and the concentration of the iodine/cyclohexane solution display an excellent linear relationship, which can be described using the equation of $y = 0.00388x - 0.01509$, where y and x are the absorbance at 522 nm and the concentration of iodine/cyclohexane solution, respectively. As shown in Fig. S25–S32,† the absorbance at 522 nm of the iodine/cyclohexane solution obviously decreased with increasing time after **ZIF-90** and **ZIF-90-I–ZIF-90-III** were soaked in this solution, respectively, indicating that iodine was adsorbed by these materials. The residual concentration of iodine in cyclohexane can be speculated by the equation of $y = 0.00388x - 0.01509$, and the iodine adsorption values were calculated using the following equation: $Q_t = (C_0 - C_t) \times V \div m$, where Q_t (mg g^{-1}) is the iodine adsorption amount from the iodine/cyclohexane solution per gram of samples at time t, C_0 (mg L^{-1}) is the initial concentration of the iodine/cyclohexane solution, C_t (mg L^{-1}) is the concentration of the iodine/cyclohexane solution after adsorption at time t, V (mL) is the volume of iodine/cyclohexane solution, and m (mg) is the mass of the sample.

As shown in Fig. 4, S33 and Table S11,† the maximum iodine equilibrium adsorption amounts were 538, 1005, 1461 and 1826 mg g^{-1} for **ZIF-90** and **ZIF-90-I–ZIF-90-III**, respectively, and the iodine adsorption capacity of **ZIF-90-III** is 3.4-fold the value for **ZIF-90**. Similar to the iodine vapor adsorption behavior, the iodine adsorption capacity of **ZIF-90** in the iodine/cyclohexane solution was also enhanced with the increasing conversion of the aldehyde to a Schiff base, especially with increasing ratio of the mono-Schiff base. This behavior also indicates that the iodine adsorption capacity of the materials in the iodine/cyclohexane solution is not only ascribed to the suitable cage size and charge-transfer interaction between the iodine molecule and aromatic imidazole ring, but also results from the introduction of C=N and NH_2 groups with rich electrons. These factors are beneficial to forming multipoint interactions between the iodine molecule and framework, and further improving the iodine adsorption capacity of compounds. To our best knowledge, compared to the previously reported MOFs (Fig. 4 and Table S12†), the iodine adsorption values of **ZIF-90-II** and **ZIF-90-III** are lower than those for **IL@PCN-333** (Al) (3400 mg g^{-1}),[22] $Ti_{16}Pb_5O_{16}(C_6H_5CO_2)_2(OCH_3)_{40}$ (3127 mg g^{-1})[31] and Ag@MIL-101 (2140 mg g^{-1}),[32] but higher than that of most known MOFs, among the highest iodine adsorption capacity.

The pseudo-first and pseudo-second order kinetic models were also adopted to study the iodine adsorption kinetics of **ZIF-90** and **ZIF-90-I–ZIF-90-III** in the iodine/cyclohexane solution. As shown in Fig. S34–S49 and Tables S13–S16,† and according to R^2 and the calculated values of Q_e (mg g^{-1}) obtained *via* the pseudo-first and pseudo-second order kinetic equations, the pseudo-second order kinetic equation better describes the

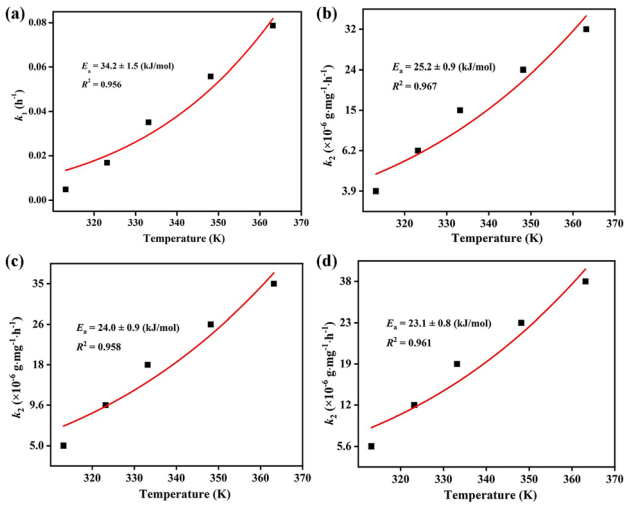

Fig. 3 Arrhenius fitting of the iodine vapor adsorption by (a) ZIF-90, (b) ZIF-90-I, (c) ZIF-90-II and (d)ZIF-90-III.

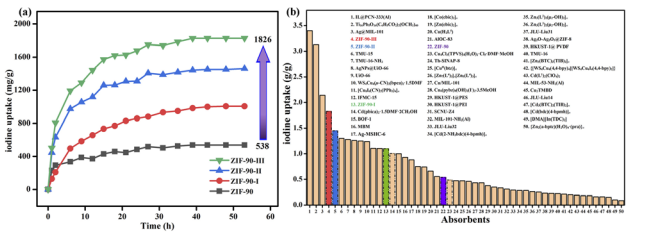

Fig. 4 (a) Iodine adsorption isotherms of ZIF-90 and ZIF-90-I–ZIF-90-III from 15 mL of 1000 mg L^{-1} iodine/cyclohexane solution, and (b) comparison of the iodine adsorption capacity from iodine solution by reported metal–organic frameworks and our materials.

iodine adsorption by **ZIF-90** and **ZIF-90-I–ZIF-90-III**, indicating that chemisorption exists in the iodine absorption progress.[33,34] Additionally, the iodine absorption isotherms of **ZIF-90** and **ZIF-90-I–ZIF-90-III** in the iodine/cyclohexane solution were also further explored *via* Langmuir and Freundlich isotherm model, respectively, and these two isotherm models are expressed by the following equations:

$$\text{Langmuir isotherm model: } Q_e = (Q_m K_L C_e)/(1 + K_L C_e)$$

$$\text{Freundlich isotherm model: } Q_e = K_F C_e^{\,1/n}$$

where Q_e (mg g^{-1}) and C_e (mg L^{-1}) are the equilibrium iodine adsorption amount and concentration of the iodine/cyclohexane solution, respectively, Q_m (mg g^{-1}) is the theoretical maximum adsorption value, K_L (L mg^{-1}) and K_F (mg g^{-1}) are the adsorption constants of Langmuir and Freundlich isotherm model, respectively, and n is the Freundlich linearity index. As shown in Fig. 5 and the related parameters obtained from the Langmuir and Freundlich isotherm models (Table S17†), the Langmuir isotherm model is in better agreement with the experimental adsorption isotherm for **ZIF-90** and **ZIF-90-I–ZIF-90-III** than the Freundlich isotherm model, indicating that the iodine adsorption process in the iodine/cyclohexane solution by these materials probably due to the monolayer chemisorption occurring on the heterogeneous surfaces.[5,33]

3.4. Characterization of iodine-loaded ZIF-90 and ZIF-90-I–ZIF-90-III

Raman spectra and XPS were carried out on pristine and iodine-loaded **ZIF-90** and **ZIF-90-I–ZIF-90-III** (including these samples that adsorbed iodine from iodine vapor and iodine/cyclohexane solution, respectively) to detect the probable species of iodine in these iodine-loaded materials, and explore the interactions between the iodine molecule and framework. As shown in Fig. 6, two strong peaks of 112 and 168 cm^{-1} were detected on the Raman spectrum of the iodine-loaded **ZIF-90** and **ZIF-90-I–ZIF-90-III**. The peak of 168 cm^{-1} may be ascribed to the iodine molecule, which was shifted by 12 cm^{-1} and is comparable to the I–I vibration of solid iodine (180 cm^{-1}) (Fig. S50†). This reveals that the adsorbed iodine molecules were bound to the framework, and probably due to the formation of hydrogen bonds between the iodine molecule and the NH_2 group from the framework or the formation of a partial dipole moment between the iodine molecule and electron-rich organic linkers with the C=N bond and aromatic ring.[34] The peak of 112 cm^{-1} probably corresponds to the I_3^- species. This may be a result from the charge transfer between the anti-bond I_2 molecular orbital and the lone pair orbital of the O/N atom from organic linkers, and the iodine molecule was subsequently polarized to form I_3^- anions.[35]

Meanwhile, the binding energies for the $3d_{5/2}$ and $3d_{3/2}$ orbitals of iodine theoretically are 620.1 and 630.6 eV, respectively, and the binding energies will slightly shift due to the host–guest interaction. As shown in Fig. 7, two couples binding energies were observed by XPS of the iodine-loaded **ZIF-90** and **ZIF-90-I–ZIF-90-III**. The binding energies of 620.6 and 632.0 eV probably are ascribed to the iodine molecules, and the binding energies of 619.0 (619.1) and 630.4 (630.5) eV probably occur because of the existence of the I_3^- species.[36] Thus, both Raman spectra and XPS suggested that both I_2 and I_3^- species existed in the iodine-loaded **ZIF-90** and its post-synthetic derivatives. The production of the I_3^- species also proved that chemical adsorption occurred in the process of iodine adsorption from iodine vapor and iodine/cyclohexane solution by these mentioned materials, further confirming the formation of charge-transfer compounds between the iodine molecule and aromatic ring.[11–13]

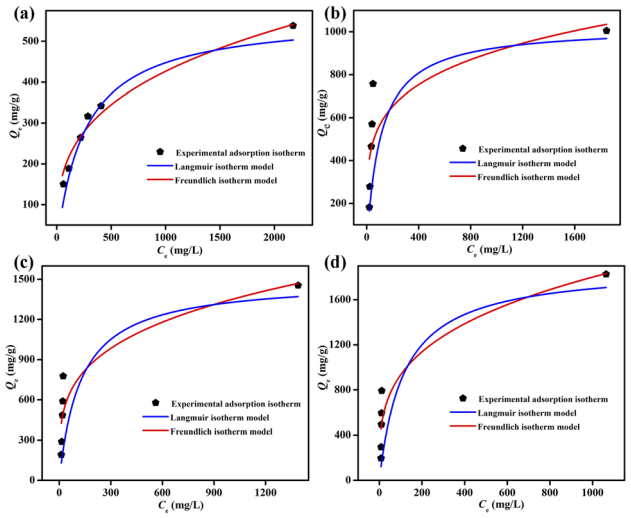

Fig. 5 The fitting of the iodine adsorption isotherms adopting the Langmuir and Freundlich isotherm models for (a) ZIF-90, (b) ZIF-90-I, (c) ZIF-90-II and (d) ZIF-90-III. High C_e values were approximatively obtained using the adsorption data of 15 mL iodine/cyclohexane solution with different concentrations.

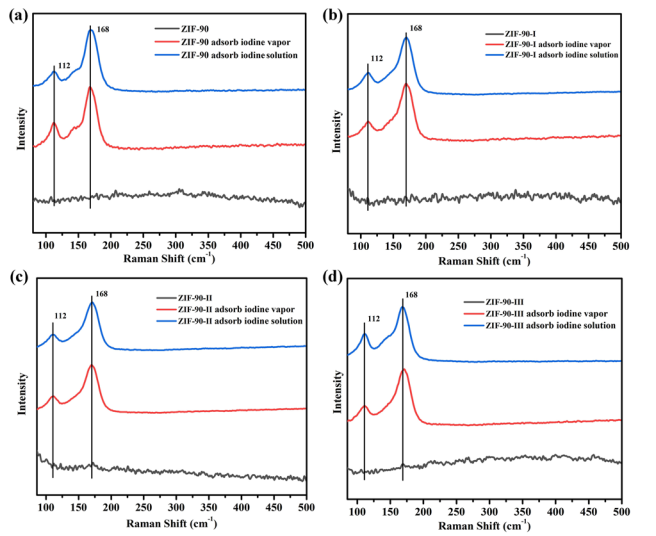

Fig. 6 Raman spectra of the pristine and iodine-loaded (a) ZIF-90, (b) ZIF-90-I, (c) ZIF-90-II and (d) ZIF-90-III.

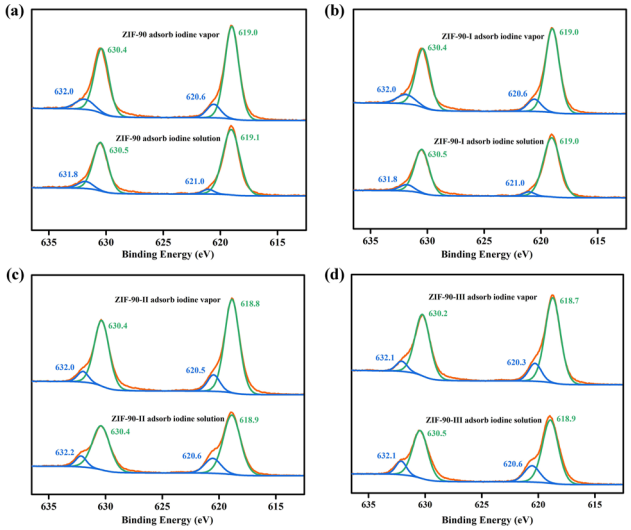

Fig. 7 XPS of the iodine-loaded (a) ZIF-90, (b) ZIF-90-I, (c) ZIF-90-II and (d) ZIF-90-III.

3.5. Theoretical insight into the iodine molecule adsorption of ZIF-90 and ZIF-90-I–ZIF-90-III

Taking the characteristic of the multicomponent structure of **ZIF-90-I–ZIF-90-III** into consideration, it is difficult to directly analyze the interactions between iodine and **ZIF-90-I–ZIF-90-III**. So many efforts have been carried out on synthesizing single crystals of **ZIF-90** with pure mono-Schiff base (**ZIF-90-mono**), **ZIF-90** with pure bis-Schiff base (**ZIF-90-bis**) and **ZIF-90** with mono-Schiff base and bis-Schiff base (**ZIF-90-mono-bis**). Unfortunately, no corresponding crystals were gained. Therefore, we performed density functional theory (DFT) calculations[37,38] with Gaussian 16 A.03 program[39] to investigate the interactions between iodine and compounds **ZIF-90-mono**/**ZIF-90-bis** based on the cluster model.[40,41] The geometry optimizations and electronic structure calculations were implemented at the PBE1PBE level[42] with GD3BJ dispersion corrections.[43] The def2-TZVPD basis set[44] was adopted for Zn and I atoms, while the 6-31++G(d,p) basis set was used for other atoms. In order to further improve the computational efficiency, the diaminocyclohexane molecules were replaced by NH_3 to generate one side-edge Schiff base in the studied clusters. The final optimized clusters for **ZIF-90-mono** and **ZIF-90-bis** are shown in Fig. S51.† The binding energy (ΔE) for an iodine molecule loaded on the specified cluster can be expressed as

$$\Delta E = E_{\text{composite}} - E_{\text{I}_2} - E_{\text{cluster}}$$

where $E_{\text{composite}}$ is the energy of an iodine molecule absorbed on the specified cluster, and E_{I_2} and E_{cluster} are the energies of an iodine molecule and the specified cluster, respectively. In addition, the Mulliken charges[45] were adopted to evaluate the charge transfers between the clusters and iodine molecules.

As shown in Fig. S52,† I_2 is adjacent with the aldehyde groups from imidazole-2-carboxaldehyde in the iodine-loaded **ZIF-90**, and the relatively short I…framework distances ranged from 2.775 to 3.890 Å. In the iodine-loaded **ZIF-90-mono**, I_2 approaches a $-NH_2$ group from an individual diaminocyclohexane molecule, as well as near the imidazole and cyclohexane rings. The distances between I and these groups are in the range of 2.947–3.349 Å. In the iodine-loaded **ZIF-90-bis**, I_2 is close to the imidazole rings from the bis-Schiff base, and the longer distances of 3.146 and 3.996 Å exist between iodine and the framework. Meanwhile, the I–I distances are 2.674, 2.659 and 2.656 Å in the iodine-loaded **ZIF-90**, **ZIF-90-mono** and **ZIF-90-bis**, respectively, slightly longer than the distance of the free iodine molecule optimized at the PBE1PBE/def2-TZVPD level (2.654 Å), revealing that affinities exist in these frameworks and iodine atom. As listed in Table S18,† the transferred charges from **ZIF-90**, **ZIF-90-mono** and **ZIF-90-bis** to the iodine molecule are −0.172, −0.183 and −0.134*e*, respectively. The binding energies between the iodine molecule and the abovementioned compounds are −0.664, −0.687 and −0.574 eV, respectively, implying that the strongest interaction may be generated between **ZIF-90-mono** and the iodine molecule, while the weakest affinity probably formed between **ZIF-90-bis** and the iodine molecule. Based on these calculation results, we speculate that materials with a higher ratio of mono-Schiff base and lower ratio of bis-Schiff base will generate stronger binding forces between iodine and the framework, further leading to a higher iodine uptake capacity for these materials. This deduction is consistent with the aforementioned iodine adsorption experiments, in which **ZIF-90-III** with the highest amount of mono-Schiff bases has the maximum iodine uptake capacity, and also matches well with the subsequent iodine release from iodine-loaded materials.

3.6. Iodine release from iodine-loaded ZIF-90 and ZIF-90-I–ZIF-90-III

In order to probe the reversibility of **ZIF-90** and **ZIF-90-I–ZIF-90-III**, the iodine desorption experiments of these iodine-loaded materials (including these samples adsorbed iodine from iodine vapor and iodine/cyclohexane solution) were performed *via* heating at 120 °C, respectively. The iodine desorption capacity was estimated by the equation of $R\% = (m'_0 - m'_t)/m'_0$, where $R\%$ is the iodine release from the iodine-loaded material at time t, m'_0(mg) is the initial mass of the iodine-loaded material and m'_t(mg) is the mass of the iodine-loaded material after desorption at time t. As shown in Fig. S53,† the release rate of iodine was very fast in the initial first hour and then it became slow. Finally, the desorption approached the equilibrium after 2 hours with a recovery rate of 93.1%, 85.1%, 82.6% and 80.7% for the iodine-loaded **ZIF-90** and **ZIF-90-I–ZIF-90-III** with iodine coming from iodine vapor, and the recovery rate of 94.2%, 87.2%, 84.8% and 82.7% for iodine-loaded **ZIF-90** and **ZIF-90-I–ZIF-90-III** with iodine coming from iodine/cyclohexane, respectively. This phenomenon implied that strong interactions existed between iodine and the framework, and the sequence of the interactions between iodine and the framework is **ZIF-90-III** > **ZIF-90-II** > **ZIF-90-I** > **ZIF-90**, which is consistent with the theoretical calculation. The next iodine adsorption process cycle was carried out when one

desorption process finished. After three cycles of the adsorption–desorption process, the iodine adsorption capacity of iodine vapor by **ZIF-90** and **ZIF-90-I–ZIF-90-III** still retained a high adsorption amount of 4290, 4990, 5490, and 6450 mg g^{-1}, corresponding to 95.6%, 94.7%, 96.7% and 97.7% of their initial capacity, respectively (Fig. S54†). It is noteworthy that the iodine adsorption capacities of **ZIF-90-I–ZIF-90-III** after three cycles is still superior to the initial **ZIF-90** and only lower than the best iodine adsorption MOF material IL@PCN-333(Al),[22] still being among the highest iodine adsorption values. Meanwhile, after three cycles of the adsorption–desorption process, the retained iodine adsorption capacities from the iodine/cyclohexane solution by **ZIF-90** and **ZIF-90-I–ZIF-90-III** were 489, 897, 1288, and 1695 mg g^{-1}, corresponding to 90.9%, 89.3%, 88.2% and 92.8% of their initial capacities, respectively (Fig. S55†). Furthermore, the iodine adsorption amount of **ZIF-90-III** was still ranked in the front of MOFs with iodine trap properties from the iodine solution. Additionally, PXRD patterns of the recovered **ZIF-90** and **ZIF-90-I–ZIF-90-III** were carried out (Fig. S56†), and matched well with those of the as-synthesized ones. This indicated that these materials still kept their structures and crystallinity, further confirming the good stability and renewability of **ZIF-90** and these **ZIF-90** post-synthetic derivatives.

4 Conclusions

In conclusion, we synthesized a series of **ZIF-90** derivatives with rich electrons *via* post-synthetic modification, and the aldehyde group of **ZIF-90** was quantitatively converted to mono- and di-Schiff bases. Iodine adsorption experiments revealed that the uptake capacities of the **ZIF-90** derivatives are superior to that of **ZIF-90**. Among these **ZIF-90** derivatives, **ZIF-90-III** showed the maximum iodine adsorption capacity of 6600 mg g^{-1} and 1826 mg g^{-1} for iodine vapor and iodine/cyclohexane solution, respectively, being among the highest known to date for metal–organic frameworks. The values of the activation energies are 34.2 ± 1.5, 25.2 ± 0.9, 24.0 ± 0.9 and 23.1 ± 0.8 kJ mol^{-1} for **ZIF-90** and **ZIF-90-I–ZIF-90-III**, respectively, and the iodine adsorption kinetics of the **ZIF-90** and **ZIF-90** derivatives were investigated in detail. Meanwhile, both I_2 and I_3^- were observed in iodine-loaded **ZIF-90** and **ZIF-90** derivatives by XPS and Raman measurements. The renewable experiments indicated that our synthesized **ZIF-90** derivatives still can retain high iodine adsorption values after three cycles. This research broadens the materials with high iodine adsorption properties, and provides a good method for the improvement of iodine…framework interactions, which is beneficial to developing more iodine trap materials.

Author contributions

Z. Zhang prepared and characterized **ZIF-90** and its derivates, and analysed the data; Y. Chen and Y. Sun carried out the iodine adsorption experiments; Z.-Y. Zhang performed the theoretical calculation. F. Liang discussed the results of the theoretical calculation. Z. Chen and H.-C. Hu guided this research and wrote the manuscript. All authors commented on the manuscript.

Conflicts of interest

There are no conflicts to declare.

Acknowledgements

This work was supported by the National Natural Science Foundation of China (Grant No. 22261007, 12064002 and 22061004) and Guangxi Technology Base and Talent Subject (No. GUIKE AD23026067).

Notes and references

1 P. C. Burns, R. C. Ewing and A. Navrotsky, Nuclear fuel in a reactor accident, *Science*, 2012, **335**, 1184–1188.
2 X. Zhang, J. Maddock, T. M. Nenoff, M. A. Denecke, S. Yang and M. Schröder, Adsorption of iodine in metal–organic framework materials, *Chem. Soc. Rev.*, 2022, **51**, 3243–3262.
3 T. Pan, K. Yang, X. Dong and Y. Han, Adsorption-based capture of iodine and organic iodides: status and challenges, *J. Mater. Chem. A*, 2023, **11**, 5460–5475.
4 W. Xie, D. Cui, S.-R. Zhang, Y.-H. Xu and D.-L. Jiang, Iodine capture in porous organic polymers and metal–organic frameworks materials, *Mater. Horiz.*, 2019, **6**, 1571–1595.
5 M. Avais and S. Chattopadhyay, Porous polyaminoamides via an exotemplate synthesis approach for ultrahigh multimedia iodine adsorption, *J. Mater. Chem. A*, 2022, **10**, 20090–20100.
6 J. Chang, H. Li, J. Zhao, X. Guan, C. Li, G. Yu, V. Valtchev, Y. Yan, S. Qiu and Q. Fang, Tetrathiafulvalene-based covalent organic frameworks for ultrahigh iodine capture, *Chem. Sci.*, 2021, **12**, 8452–8457.
7 L. Xie, Z. Zheng, Q. Lin, H. Zhou, X. Ji, J. L. Sessler and H. Wang, Calix[4]pyrrole-based crosslinked polymer networks for highly effective iodine adsorption from water, *Angew. Chem., Int. Ed.*, 2022, **61**, e202113724.
8 B. Azambre, M. Chebbi, O. Leroy and L. Cantrel, Effects of zeolitic parameters and irradiation on the retention properties of silver zeolites exposed to molecular iodine, *Ind. Eng. Chem. Res.*, 2018, **57**, 1468–1479.
9 X. He, L. Chen, X. Xiao, Y. Gan, J. Yu, J. Luo, H. Dan, Y. Wang, Y. Ding and T. Duan, Improved utilization of Cu0 for efficient adsorption of iodine in gas and solution by mesoporous Cu0-SBA-15 via solvothermal reduction method, *Chem. Eng. J.*, 2023, **462**, 142175.
10 S. Yao, W.-H. Fang, Y. Sun, S.-T. Wang and J. Zhang, Mesoporous assembly of aluminum molecular rings for iodine capture, *J. Am. Chem. Soc.*, 2021, **143**, 2325–2330.
11 C. Liu, Y. Jin, Z. Yu, L. Gong, H. Wang, B. Yu, W. Zhang and J. Jiang, Transformation of porous organic cages and covalent organic frameworks with efficient iodine vapor capture performance, *J. Am. Chem. Soc.*, 2022, **144**, 12390–12399.
12 D. F. Sava, M. A. Rodriguez, K. W. Chapman, P. J. Chupas, J. A. Greathouse, P. S. Crozier and T. M. Nenoff, Capture of

volatile iodine, a gaseous fission product, by zeolitic imidazolate framework-8, *J. Am. Chem. Soc.*, 2011, **133**, 12398–12401.

13 J. T. Hughes, D. F. Sava, T. M. Nenoff and A. Navrotsky, Thermochemical evidence for strong iodine chemisorption by ZIF-8, *J. Am. Chem. Soc.*, 2013, **135**, 16256–16259.

14 Y. Lei, G. Zhang, Q. Zhang, L. Yu, H. Li, H. Yu and Y. He, Visualization of gaseous iodine adsorption on single zeolitic imidazolate framework-90 particles, *Nat. Commun.*, 2021, **12**, 4483.

15 M. Leloire, C. Walshe, P. Devaux, R. Giovine, S. Duval, T. Bousquet, S. Chibani, J. F. Paul, A. Moissette, H. Vezin, P. Nerisson, L. Cantrel, C. Volkringer and T. Loiseau, Capture of gaseous iodine in isoreticular zirconium-based UiO-n metal-organic frameworks: influence of amino functionalization, DFT calculations, Raman and EPR spectroscopic investigation, *Chem. – Eur. J.*, 2022, **28**, e202104437–e202104453.

16 P. Chen, X. He, M. Pang, X. Dong, S. Zhao and W. Zhang, Iodine capture using Zr-based metal–organic frameworks (Zr-MOFs): adsorption performance and mechanism, *ACS Appl. Mater. Interfaces*, 2020, **12**, 20429–20439.

17 J. Wang, L. Wang, Y. Wang, F. Yang, J. Li, X. Guan, J. Zong, F. Zhou, J. Huang and Y.-N. Liu, Covalently connected core-shell NH2-UiO-66@Br-COFs hybrid materials for CO2 capture and I2 vapor adsorption, *Chem. Eng. J.*, 2022, **438**, 135555.

18 W. Morris, C. J. Doonan, H. Furukawa, R. Banerjee and O. M. Yaghi, Crystals as molecules: postsynthesis covalent functionalization of zeolitic imidazolate frameworks, *J. Am. Chem. Soc.*, 2008, **130**, 12626–12627.

19 P. Kupser, K. Pagel, J. Oomens, N. Polfer, B. Koksch, G. Meijer and G. von. Helden, Amide-I and -II vibrations of the cyclic β-sheet model peptide gramicidins in the gas phase, *J. Am. Chem. Soc.*, 2010, **132**, 2085–2093.

20 A. K. Eckhardt and P. R. Schreiner, Spectroscopic evidence for aminomethylene (H–C–NH2) – the simplest amino carbine, *Angew. Chem., Int. Ed.*, 2018, **57**, 5248–5252.

21 B. Ghalei, K. Wakimoto, C. Y. Wu, A. P. Isfahani, T. Yamamoto, K. Sakurai, M. Higuchi, B. K. Chang, S. Kitagawa and E. Sivaniah, Rational tuning of zirconium metal–organic framework membranes for hydrogen purification, *Angew. Chem., Int. Ed.*, 2019, **58**, 19034–19040.

22 Y. Tang, H. Huang, J. Li, W. Xue and C. Zhong, IL-induced formation of dynamic complex iodide anions in IL@MOF composites for efficient iodine capture, *J. Mater. Chem. A*, 2019, **7**, 18324–18329.

23 B. Qi, Y. Liu, T. Zheng, Q. Gao, X. Yan, Y. Jiao and Y. Yang, Highly efficient capture of iodine by Cu/MIL-101, *J. Solid State Chem.*, 2018, **258**, 49–55.

24 B. Guo, F. Li, C. Wang, L. Zhang and D. Sun, A rare (3,12)-connected zirconium metal–organic framework with efficient iodine adsorption capacity and pH sensing, *J. Mater. Chem. A*, 2019, **7**, 13173–13179.

25 K. M. A. Qasem, S. Khan, M. N. Ahamad, H. A. M. Saleh, M. Ahmad and M. Shahid, Radioactive iodine capture by metal organic frameworks in liquid and vapour phases: an experimental, kinetic and mechanistic study, *J. Environ. Chem. Eng.*, 2021, **9**, 106720.

26 B. Liu, X. Ren, L. Chen, X. Ma, Q. Chen, Q. Sun, L. Zhang, P. Si and L. Ci, High efficient adsorption and storage of iodine on S, N co-doped graphene aerogel, *J. Hazard. Mater.*, 2019, **373**, 705–715.

27 Z. J. Li, Y. Ju, Y. Ju, B. Yu, X. Wu, H. Lu, Y. Li, J. Zhou, X. Guo, Z. H. Zhang, J. Lin, J. Q. Wang, J. Q. Wang and S. Wang, Modulated synthesis and isoreticular expansion of Th-MOFs with record high pore volume and surface area for iodine adsorption, *Chem. Commun.*, 2020, **56**, 6715–6718.

28 Z. Changani, A. Razmjou, A. Taheri-Kafrani, M. E. Warkiani and M. Asadnia, Surface modification of polypropylene membrane for the removal of iodine using polydopamine chemistry, *Chemosphere*, 2020, **249**, 126079.

29 M. Al-Ghouti, M. A. M. Khraisheh, M. N. M. Ahmad and S. Allen, Thermodynamic behaviour and the effect of temperature on the removal of dyes from aqueous solution using modified diatomite: a kinetic study, *J. Colloid Interface Sci.*, 2005, **287**, 6–13.

30 V. Vaid and R. Jindal, An efficient pH-responsive kappa-carrageenan/tamarind kernel powder hydrogel for the removal of brilliant green and rose bengal from aqueous solution, *J. Appl. Polym. Sci.*, 2022, **139**, e52218.

31 A. Said, C. Gao, C. Liu, H. Niu, D. Wang, Y. Liu, L. Du, C. H. Tung and Y. Wang, A mesoporous lead-doped titanium oxide compound with high performance and recyclability in I_2 uptake and photocatalysis, *Inorg. Chem.*, 2022, **61**, 586–596.

32 P. Mao, B. Qi, Y. Liu, L. Zhao, Y. Jiao, Y. Zhang, Z. Jiang, Q. Li, J. Wang, S. Chen and Y. Yang, Highly efficient capture of iodine by Cu/MIL-101, *J. Solid State Chem.*, 2016, **237**, 274–283.

33 S. Sun, X. Sha, J. Liang, G. Yang, X. Hu, Z. He, M. Liu, N. Zhou, X. Zhang and Y. Wei, Rapid synthesis of polyimidazole functionalized MXene via microwave-irradiation assisted multi-component reaction and its iodine adsorption performance, *J. Hazard. Mater.*, 2021, **420**, 126580.

34 C. Liu, W. Li, Y. Liu, H. Wang, B. Yu, Z. Bao and J. Jiang, Porous organic cages for efficient gas selective separation and iodine capture, *Chem. Eng. J.*, 2022, **428**, 131129.

35 K. Cheng, H. Li, J.-R. Wang, P.-Z. Li and Y. Zhao, From supramolecular organic cages to porous covalent organic frameworks for enhancing iodine adsorption capability by fully exposed nitrogen-rich sites, *Small*, 2023, 2301998.

36 H.-J. Noh, Y.-K. Im, S.-Y. Yu, J.-M. Seo, J. Mahmood, T. Yildirim and J.-B. Baek, Vertical two-dimensional layered fused aromatic ladder structure, *Nat. Commun.*, 2020, **11**, 2021.

37 W. Kohn and L. J. Sham, Self-consistent equations including exchange and correlation effects, *Phys. Rev.*, 1965, **140**, A1133.

38 R. G. Parr and W. Yang, *Density-Functional Theory of Atoms and Molecules*, Oxford Univ. Press, Oxford, 1989.

39 M. J. Frisch, G. W. Trucks, H. B. Schlegel, G. E. Scuseria, M. A. Robb, J. R. Cheeseman, G. Scalmani, V. Barone,

G. A. Petersson, H. Nakatsuji, X. Li, M. Caricato, A. V. Marenich, J. Bloino, B. G. Janesko, R. Gomperts, B. Mennucci, H. P. Hratchian, J. V. Ortiz, A. F. Izmaylov, J. L. Sonnenberg, D. Williams-Young, F. Ding, F. Lipparini, F. Egidi, J. Goings, B. Peng, A. Petrone, T. Henderson, D. Ranasinghe, V. G. Zakrzewski, J. Gao, N. Rega, G. Zheng, W. Liang, M. Hada, M. Ehara, K. Toyota, R. Fukuda, J. Hasegawa, M. Ishida, T. Nakajima, Y. Honda, O. Kitao, H. Nakai, T. Vreven, K. Throssell, J. A. Montgomery Jr, J. E. Peralta, F. Ogliaro, M. J. Bearpark, J. J. Heyd, E. N. Brothers, K. N. Kudin, V. N. Staroverov, T. A. Keith, R. Kobayashi, J. Normand, K. Raghavachari, A. P. Rendell, J. C. Burant, S. S. Iyengar, J. Tomasi, M. Cossi, J. M. Millam, M. Klene, C. Adamo, R. Cammi, J. W. Ochterski, R. L. Martin, K. Morokuma, O. Farkas, J. B. Foresman and D. J. Fox, *Gaussian*, Wallingford CT, 2016.

40 L. Grajciar, O. Bludský and P. Nachtigall, Water adsorption on coordinatively unsaturated sites in CuBTC MOF, *J. Phys. Chem. Lett.*, 2010, **1**, 3354–3359.

41 P. Chen, X. He, M. Pang, X. Dong, S. Zhao and W. Zhang, Iodine capture using Zr-Based metal–organic Frameworks (ZrMOFs): adsorption performance and mechanism, *ACS Appl. Mater. Interfaces*, 2020, **12**, 20429–20439.

42 C. Adamo and V. Barone, Toward reliable density functional methods without adjustable parameters: the PBE0 model, *J. Chem. Phys.*, 1999, **110**, 6158–6170.

43 S. Grimme, S. Ehrlich and L. Goerigk, Effect of the damping function in dispersion corrected density functional theory, *J. Comput. Chem.*, 2011, **32**, 1456–1465.

44 D. Rappoport and F. Furche, Property-optimized Gaussian basis sets for molecular response calculations, *J. Chem. Phys.*, 2010, **133**, 134105.

45 R. S. Mulliken, Electronic population analysis on LCAO-MO molecular wave functions, *J. Chem. Phys.*, 1955, **23**, 1833–1840.